Zegers, E.J.P., Williams, B.A., Sheinson, R.S., and Fleming, J.W., "Water Mist Suppression of Non-Premixed Counterflow Flames," ***Proceedings of the Fall Technical Meeting of the Eastern States Section of the Combustion Institute*****, Raleigh, pp. 109-112, 1999.**

Water Mist Suppression of Non-Premixed Counterflow Flames

E.J.P. Zegers[1], B.A. Williams, R.S. Sheinson, and J.W. Fleming[2]
Combustion Dynamics Section, Code 6185, Chemistry Division
Naval Research Laboratory, Washington, DC 20375-5342 USA

[1] National Research Council Postdoctoral Fellow (1997-1999).
[2] Corresponding author: fleming@code6185.nrl.navy.mil .

Introduction

Water mists possess many attributes of the ideal fire suppressant. They are non-toxic, non-corrosive, and have zero ozone depletion and global warming potentials. Water mists also offer significant cooling capacity, due to the heat of vaporization associated with water in the liquid phase. Conventional sprinkler systems typically produce sprays of droplets with diameters on the order of 800 μm. Mists differ from sprays in that they are composed of droplets with diameters below 200 μm. The small droplet size leads to larger surface to volume ratios and longer suspension times, improving water vaporization in the fire. Less water is therefore required to extinguish the flames, and the liquid water residue is minimized. Small droplets also follow the combustion gases more closely, and have the capability of reaching obstructed areas. These attributes have prompted the U.S. Navy to adopt water mist systems as replacements for Halon 1301 systems, in machinery space total flooding applications aboard certain classes of ships.

Nevertheless, the nature of the interaction between water mists and flames has not been fully investigated. Mists extinguish flames mainly by increasing the heat capacity of the reactant streams. Water in the vapor phase also dilutes the reactants. The behavior of the droplets in the combustion flow field dictates where the droplets evaporate, the impact they have on the reaction zone, whether they evaporate completely or not, and thus the effectiveness of the mist. A better understanding of the relationship between mist droplet size, concentration, droplet evolution in the flow field, and flame extinction will guide water mist system optimization. Lentati and Chelliah (1998a, 1998b) investigate this relationship numerically, by modeling the behavior of water mists in methane/air counterflow flames. In the present study, the relationship is investigated through water mist experiments in non-premixed counterflow propane/air flames.

Experimental Setup

The counterflow burner used to conduct the water mist experiments has been described previously (Papas, 1996; Zegers, 1999). Fig. 1 shows a diagram of the burner setup. Propane flows from the top tube. The mist is supplied in the air stream from the bottom tube. The tubes are housed in a Plexiglas chamber, which is continuously purged with nitrogen. Both tubes have inner diameters of 10 mm, and are 10 mm apart. For gaseous reactants in this configuration, a relationship exists between the local strain rate imposed on the flame and the global strain rate, calculated from burner gap size and reactant velocities and densities (Fisher, 1997). This burner specific relationship is used in the present study to calculate local strain rates. The relationship provides the local strain rate that would be imposed on the flame if the mist were not present.

The mists are produced using a TSI Inc. model 3450 Vibrating Orifice Aerosol Generator (VOAG), based on the design of Berglund and Liu (1973). Water is forced through a pinhole that is piezoelectrically excited. At specific resonant frequencies, the water jet breaks up into a monodisperse droplet stream. This stream exits the generator through a hole in the dispersion cap. By forcing air to exit through this same hole, the droplet stream is dispersed into a cloud as it exits the droplet generator and enters the counterflow burner's bottom tube. The aerosol then mixes with a secondary air stream when additional air flow is needed, and the mixture proceeds up the tube to the reaction zone. Using a 5 μm diameter pinhole, monodisperse droplet streams with a size distribution peak at diameters of 14, 18, or 24 μm have been produced. With a 10 μm diameter pinhole, monodisperse streams of 25, 30, and 37 μm droplets have been obtained.

The evolution of the mists in the counterflow field is studied using Phase Doppler Particle Anemometry. Based on this technique, droplet diameters, axial velocities and number densities are measured at discreet points in the field. The PDA beams enter, and the light scattered by the particles exits the Plexiglas chamber through optical windows. The burner lies on a translation stage, such that the PDA probe volume can be positioned anywhere in the gap between the opposed tubes. In the present investigation, the axial position of the flame is determined by centering the PDA probe volume in the middle of the flame's visible emission zone.

Results

Droplet Behavior

Figures 2a and 2b show the size distribution evolution, in propane/air counterflow flames, of 30 and 18 μm mists respectively. The figures provide the number densities of the various size droplets in the flow as a function of axial position (x), along the burner's axis (r = 0 mm). The local strain rate (K) imposed on the flames corresponds to approximately 30% of the extinction strain rate for the uninhibited flame ($K_{ext} = 608\ s^{-1}$). The air and droplets exit the lower tube at x = 0 mm; the propane exits the upper tube at x = 10 mm. The flames are located at x = 5 and 4.5 mm, in the 30 and 18 μm mist experiments respectively. In both cases, the diameter of the droplets changes very little before the flame is reached, with the 30 or 18 μm droplets dominating the size distribution. In the flame region, the droplets evaporate, and the peak in the size distribution shifts to smaller diameters. Very few droplets are detected 2 mm after the flame.

Figures 3a and 3b focus specifically on the number density profiles of the 30 and 18 μm droplets respectively. Number density is plotted versus axial position. In both experiments, the density first increases with axial position; then quickly drops in the flame region. Three effects combine to explain the shape of the number density profiles.

The main effect is related to the velocity profiles of the 30 and 18 μm droplets, provided in Figs. 3a and 3b respectively. At the lower tube exit, the droplets have roughly the same velocity as the gas stream. As the gas stream's axial velocity changes in the counterflow field, the equilibrium in velocity between the liquid and gas phases is lost, and the drag forces act to reestablish it. The droplet velocity profile therefore follows that of the gases: the velocity initially drops as the gases move towards the stagnation plane; it then increases when the hot gases expand in the reaction zone, before it drops down again, close to the stagnation plane. In regions where the droplets are decelerating, faster droplets catch up to slower ones, and the number density will tend to rise. In the flame region, the droplets accelerate, which tends to reduce their number density. Figures 3a and 3b show that the impact of axial velocity gradients on droplet number density is significant, with variations in number density well correlated with variations in velocity.

Furthermore, as the air exits the lower tube, the flow streamlines begin to diverge in the counterflow field, producing radial drag forces on the mist. Due to this effect, the droplets move away from the burner axis. The divergence of the air flow therefore acts to reduce the droplet number density along the centerline. The third effect is evaporation in the flame region, which causes the droplet size to decrease, and thus also contributes to the decrease in the number densities of the 30 and 18 μm droplets.

The suppression effectiveness of a mist depends more on the flux of droplets to the flame than the number density. Figures 4a and 4b show droplet flux profiles for the 30 and 18 μm mist experiments, respectively. The fluxes are normalized by the maximum value measured at x = 2 mm: 48.2×10^3 and 177.5×10^3 droplets/s/cm^2 for the 30 and 18 μm mist experiments, respectively. The droplet flux decreases as the flame is approached, under the effects of the diverging flow and evaporation. The scatter in the data is attributable in part to experimental uncertainties, in the PDA concentration measurements in particular. Slight variations in the position of the flame over the course of the experiment also contribute to the scatter.

Flame Extinction

The suppression effectiveness of the 30 μm mist was investigated at two different loadings in a non-premixed propane/air counterflow flame. Droplet fluxes were measured on the burner axis, at x = 2 mm and a strain rate within 10% of extinction. For water mist fluxes of 1.66 and 2.48 $\mu l/s/cm^2$, extinction strain rates of 354 and 267 s^{-1} are obtained, respectively. At these strain rates, the water extinction mass fractions are 2.4 and 4.5%, compared to Halon 1301 extinction mass fractions of 3.7 and 6.5% respectively (Zegers, 1999). These results are summarized in table 1.

Conclusions

Using piezoelectric generation of aerosol droplets, the behavior of 30 and 18 μm mists in non-premixed propane/air counterflow flames was investigated. For both size mists, the peak in the droplet size distribution does not change until the flame zone is reached. The peak then shifts to smaller diameters due to evaporation. Variations in number density with axial position are strongly correlated with variations in droplet axial velocity. 30 and 18 μm droplet fluxes drop between the air tube exit and the stagnation plane, due to the effects of the diverging flow and evaporation. For both 30 and 18 μm mists, very few droplets survive the flame, suggesting that, for these size droplets, in a counterflow flame at moderate strain rate, most of the suppression potential of the mist is being used.

On a mass basis, a 30 micron mist was found to be more effective than Halon 1301 at suppressing non-premixed propane/air counterflow flames, at strain rates of 44 and 58% of the uninhibited flame extinction strain rate. Experiments are currently being conducted to study 30 micron mist suppression at lower strain rates. Mist sizes other than 30 μm are also being investigated.

This research is sponsored by the US Department of Defense's Next Generation Fire Suppression Technology Program funded by the DoD Strategic Environmental Research and Development Program.

References

Berglund, R.N., and Liu, B.Y.H. (1973) *Env. Sci. & Tech.*, **7**, 147.

Fisher, E.M., Williams, B.A., and Fleming, J.W. (1997) *Chemical and Physical Processes in Combustion*, October 27-29, 1997, p. 191.

Lentati, A.M., and Chelliah, H.K. (1998a) *Comb. Flame*, **115**, 158.

Lentati, A.M., and Chelliah, H.K. (1998b) *Twenty-Seventh Symposium (International) on Combustion*, The Combustion Institute, Pittsburgh, p. 2839.

Papas, P., Fleming, J.W., and Sheinson, R.S. (1996) *Twenty-Sixth Symposium (International) on Combustion*, The Combustion Institute, Pittsburgh, p. 1405.

Zegers, E.J.P., Williams, B.A., Fisher, E.M., Fleming, J.W., and Sheinson, R.S. (1999) Suppression of non-premixed flames by fluorinated ethanes and propanes, submitted to *Comb. Flame*.

Table 1: 30 μm mist and Halon 1301 extinction mass fractions (%).

	Extinction Strain Rate	
Agent	**354 s^{-1}**	**267 s^{-1}**
30 μm mist	1.4*	2.7*
Halon 1301	3.7	6.0*

(*Entries corrected from Proceedings)

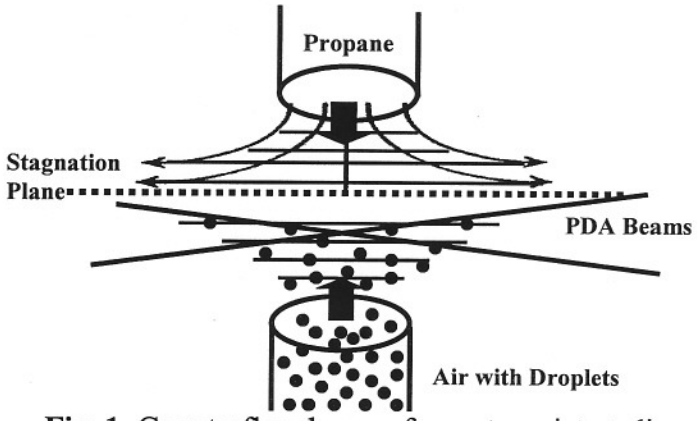

Fig. 1 Counterflow burner for water mist studies.

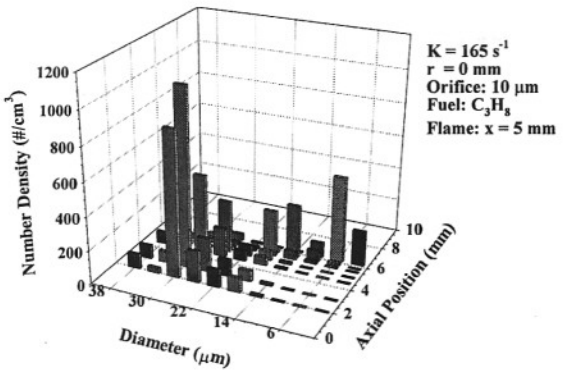

Fig. 2a Droplet size distribution evolution for 30 μm mist in propane/air counterflow flame.

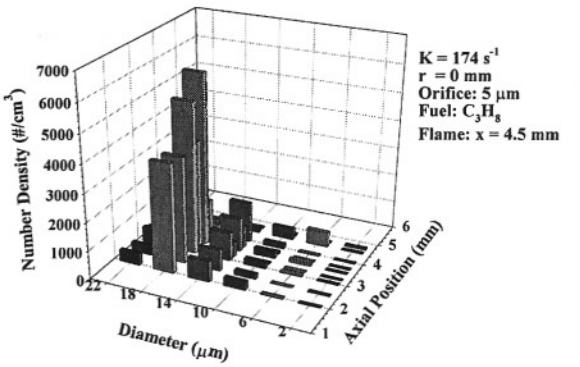

Fig. 2b Droplet size distribution evolution for 18 μm mist in propane/air counterflow flame.

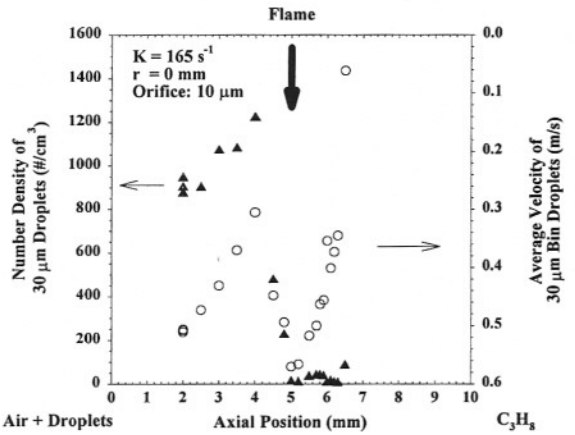

Fig. 3a Number density and velocity profiles for 30 μm droplets in propane/air/30 μm mist counterflow flame.

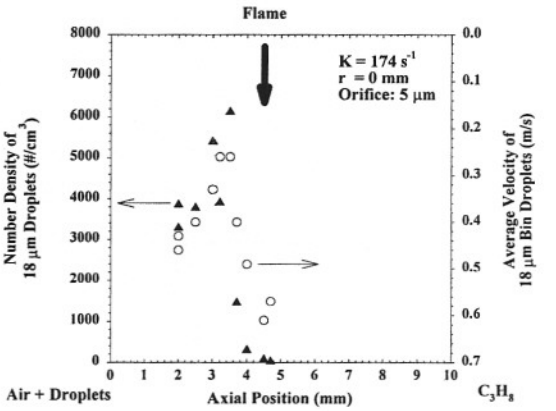

Fig. 3b Number density and velocity profiles for 18 μm droplets in propane/air/18 μm mist counterflow flame.

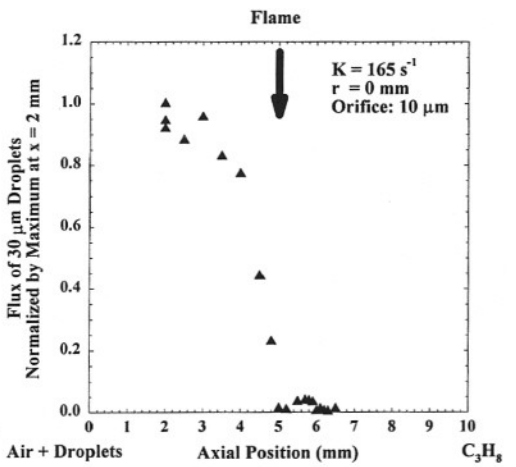

Fig. 4a 30 μm droplet flux profile for 30 μm mist in propane/air counterflow flame.

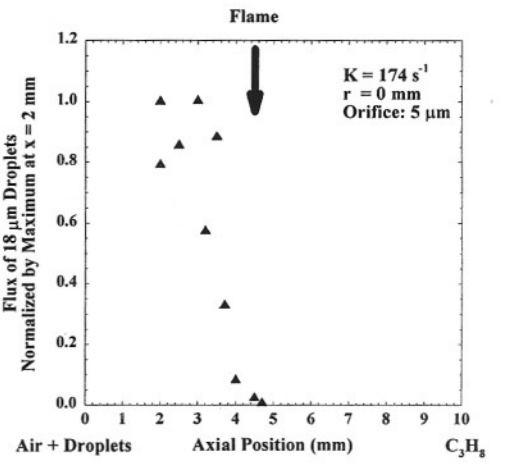

Fig. 4b 18 μm droplet flux profile for 18 μm mist in propane/air counterflow flame.